Experimental Studies of Cavity and Core Flow Interactions With Application to Ultra-Compact Combustors

Citation	Blunck, D. L., Shouse, D. T., Neuroth, C., Lynch, A., Erdmann, T. J., Burrus, D. L., ... & Caswell, A. (2014). Experimental Studies of Cavity and Core Flow Interactions With Application to Ultra-Compact Combustors. Journal of Engineering for Gas Turbines and Power, 136(9), 091505. doi:10.1115/1.4026975
DOI	10.1115/1.4026975
Publisher	American Society of Mechanical Engineers
Version	Version of Record
Terms of Use	http://cdss.library.oregonstate.edu/sa-termsofuse

David L. Blunck[1]
Air Force Research Laboratory,
Wright-Patterson AFB, OH 45433
e-mail: david.blunck@oregonstate.edu

Dale T. Shouse
Air Force Research Laboratory,
Wright-Patterson AFB, OH 45433
e-mail: dale.shouse@us.af.mil

Craig Neuroth
Air Force Research Laboratory,
Wright-Patterson AFB, OH 45433
e-mail: craig.neuroth@us.af.mil

Amy Lynch
Air Force Research Laboratory,
Wright-Patterson AFB, OH 45433
e-mail: amy.lynch.1@us.af.mil

Timothy J. Erdmann
Innovative Scientific Solutions Inc.,
Dayton, OH 45459
e-mail: timothy.erdmann.3.ctr@us.af.mil

David L. Burrus
Innovative Scientific Solutions Inc.,
Dayton, OH 45459
e-mail: david.burrus.1.ctr@us.af.mil

Joseph Zelina
GE Aviation,
Evendale, OH 45241
e-mail: joseph.zelina@ge.com

Daniel Richardson
NRC Research Associate,
Wright-Patterson AFB, OH 45433
e-mail: daniel.richardson.26.ctr@us.af.mil

Andrew Caswell
Spectral Energies, LLC,
Dayton, OH 45431
e-mail: andrew.caswell.2.ctr@us.af.mil

Experimental Studies of Cavity and Core Flow Interactions With Application to Ultra-Compact Combustors

Reducing the weight and decreasing pressure losses of aviation gas turbine engines improves the thrust-to-weight ratio and improves efficiency. In ultra-compact combustors (UCC), engine length is reduced and pressure losses are decreased by merging a combustor with adjacent components using a systems engineering approach. High-pressure turbine inlet vanes can be placed in a combustor to form a UCC. In this work, experiments were performed to understand the performance and associated physics within a UCC. Experiments were performed using a combustor operating at pressures in the range of 520–1030 kPa (75–150 psia) and inlet temperature equal to 480–620 K (865 R–1120 R). The primary reaction zone is in a single trapped-vortex cavity where the equivalence ratio was varied from 0.7 to 1.8. Combustion efficiencies and NO_x emissions were measured and exit temperature profiles were obtained for various air loadings, cavity equivalence ratios, and configurations with and without representative turbine inlet vanes. A combined diffuser-flameholder (CDF) was used to study the interaction of cavity and core flows. Discrete jets of air immediately above the cavity result in the highest combustion efficiencies. The air jets reinforce the vortex structure within the cavity, as confirmed through coherent structure velocimetry of high-speed images. The combustor exit temperature profile is peaked away from the cavity when a CDF is used. Testing of a CDF with vanes showed that combustion efficiencies greater than 99.5% are possible for $0.8 \leq \Phi_{cavity} \leq 1.8$. Temperature profiles at the exit of the UCC with vanes agreed within 10% of the average value. Exit-averaged emission indices of NO_x ranged from 3.5 to 6.5 g/kg_{fuel} for all test conditions. Increasing the air loading enabled greater mass flow rates of fuel with equivalent combustion efficiencies. This corresponds to increased vortex strength within the cavity due to the greater momentum of the air driver jets.
[DOI: 10.1115/1.4026975]

Introduction

Reducing the weight of aviation gas turbine engines and decreasing pressure losses improves the thrust-to-weight ratio and improves thermal efficiency, respectively. Decreasing the size of individual components (e.g., compressor and combustor) is one approach to reducing the size and weight of an engine. However, reductions in the size of individual components are limited by the axial length or residence time required to complete reactions or produce acceptable flows.

In ultracompact combustors (UCCs), the engine length is reduced and pressure losses are decreased by merging a combustor with adjacent components using a systems engineering approach [1–5]. Specifically, the high-pressure turbine inlet vanes, which are normally situated at the combustor exit, are integrated into the combustor [6]. Thus, the flow is turned and accelerated within the combustor prior to entering the first stage of the high-pressure turbine. UCCs have the potential to be used as main combustors or as interturbine burners (ITBs). When used as the main burner, a UCC can reduce the length of the engine, as illustrated in Fig. 1. A study has also characterized eliminating the compressor outlet guide vanes (OGV) upstream of the combustor [7]. By eliminating the OGV (i.e., 2.1 cm, 0.8 in), anchoring the reactions in a cavity, and merging the turbine inlet vane within the combustor (i.e., 5 cm, 2 in), the length of the system can be reduced to ~30.5 cm (12 in). This 30% reduction in length may decrease the weight of an engine by 2.4%, ignoring changes in the weight resulting from differences in structural requirements, nacelle, and airframe. When a UCC is used as an ITB, the length of the engine may not be reduced; however, additional energy supplied to the turbine can be used for power extraction or increased thrust [8,9].

Two types of UCCs have been reported in the literature: (1) high-g [6,10,11] and (2) trapped-vortex combustors (TVC) [12–14]. In a high-g combustor, the fuel and air are swirled in the azimuthal direction (around the engine centerline) in a cavity that is recessed from the flow. In a TVC, vortices that have an axis of

[1]Now with the School of Mechanical, Industrial, and Manufacturing Engineering at Oregon State University.

Contributed by the Combustion and Fuels Committee of ASME for publication in the Journal of Engineering for Gas Turbines and Power. Manuscript received December 19, 2013; final manuscript received January 17, 2014; published online March 26, 2014. Editor: David Wisler.

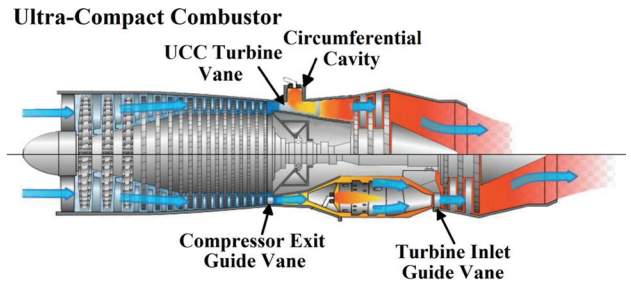

Fig. 1 Illustration of UCC (top) and conventional combustor (bottom) integrated into an engine [7]

rotation tangent to the circumference of the combustor are within a cavity. Fuel-rich combustion products migrate from the high-g or trapped-vortex cavities into the core flow, where the combustion process is completed.

Several studies have documented the fluid-mechanic interactions of the flows within a cavity and the cross stream. Sturgess and Hsu [12] quantified the entrainment of the core flow into the cavity of a TVC that results from cavity vortex motion and conservation of momentum of the fuel and air jets. Air was entrained from the cavity into the core flow for momentum ratios of the cavity with respect to the mainstream that were near 0.2. Air from the mainstream was entrained into the cavity at momentum ratios greater than ~0.3 because of pumping of the air jets in the cavity. Burguburu et al. [14] showed that the size and rotation of the vortex structures within the cavity depend on the ratio of the main and core mass flows (i.e., proportional to momentum ratios), based on particle-imaging velocimetry measurements. Further research is needed to extend this work and quantify the influence of the interaction of core and cavity flows on parameters such as combustion efficiency and pollutant emissions.

Studies have been conducted on placing vanes in the core flow above the cavity as a method of turning the flow and improving the mass transfer of exhaust products into the mainstream [3,10,15]. Regions of low pressure that form along the vanes cause the fluid in the cavity to migrate into the core flow. Sekar et al. [16] calculated the mass transfer of fluid from the cavity into the core flow for a trapped-vortex arrangement with no vanes, smooth vanes, and vanes with notches. Adding vanes to the flow improved the mixing and vorticity but increased the pressure losses by up to 6%. The addition of notches in the vanes tended to create helical spiral-vortex rings that increased the distribution of the hot exhaust into the core flow [16]. Ramps placed in the flow (instead of vanes) resulted in a temperature distribution at the exit that was more parabolic than that for configurations with vanes [5]. Experimental data are needed to validate the calculated results and provide insight into the fluid mechanics within the cavity and core flows.

The objective of this study was to provide insights into the physical and chemical processes associated with the interaction of core and cavity flows within a TVC-based UCC system. Assessments were made regarding combustor performance using measurements made of combustion efficiency, NO_x emissions, and temperature profiles for various cavity and front-end configurations.

Experimental Approach

Combustor Testing. Testing of a planar section of a UCC was performed to assess the combustion efficiency, NO_x emissions, temperature profile, and fluid mechanics within the cavity for various combustor configurations and momentum ratios. The core flow entered the front of the combustor and flowed either through one of two configurations, either around the turbine inlet vanes (see Fig. 2) or through a series of discrete air jets in the combined diffuser-flameholder (CDF) (see Fig. 3). The former configuration

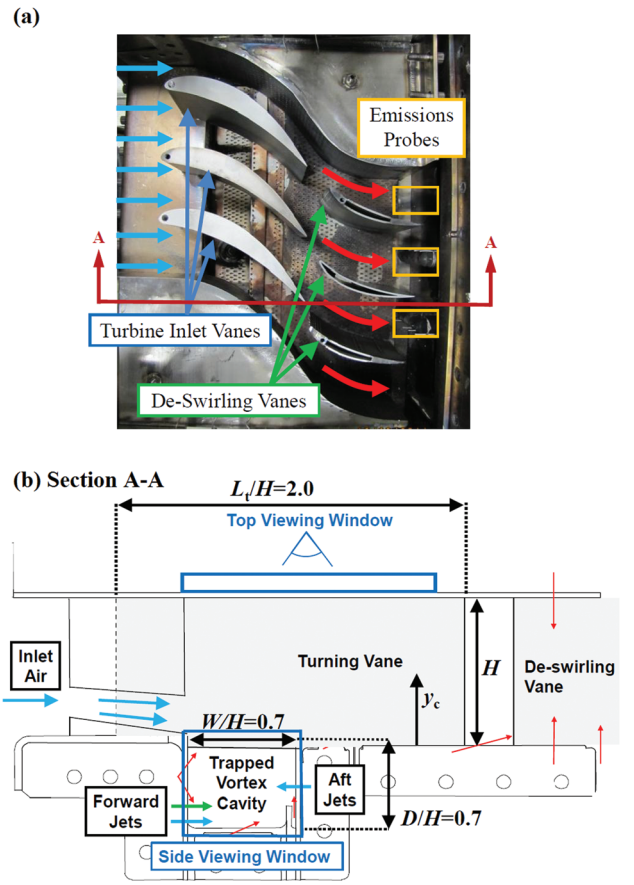

Fig. 2 UCC (side view) with CDF-2 with turbine inlet vanes above the cavity. (*a*) Photograph of top view of experimental arrangement. (*b*) Illustration of side view of combustor where air driver jets and inlets are shown in blue, fuel injectors in green, and effusion cooling in red.

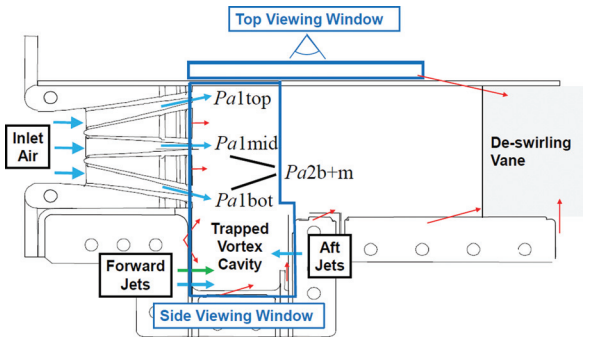

Fig. 3 UCC (side view) with CDF at the inlet to the combustor and turbine inlet vanes removed. Air from driver jets and inlets is shown in blue, fuel injectors are shown in green, and effusion cooling in red.

is representative of a UCC, while the latter was used to assess changes resulting from different air distributions between the core and cavity with no vane present. For both configurations, the fuel and air mix in the cavity, react, migrate from the cavity into the core flow (where reactions continue), and then move through the row of deswirling vanes located at the exit (see Fig. 2). The deswirling vanes were used to straighten the flow and avoid unnecessary lateral forces on the experimental arrangement. These vanes do not represent components within an engine.

Experiments were performed with the CDF located along the leading edge of the cavity (see Fig. 3) for all configurations except

when the vanes were used. Using the CDF permitted the number and height of the jets relative to the cavity to be varied. This facilitated improved understanding of the key physics associated with mass transport within and from the cavity, without the complexity of turbine inlet vanes. The CDF consisted of three rows and seven columns of discrete air passages (i.e., *Pa*), as illustrated in Fig. 3. The normalized vertical spacing between the rows of the CDF passages was $d_p/H = 0.4$. The face of the CDF and the discrete nature of the jets aided the device in serving as a flameholder for the combustion products migrating from the cavity. Various rows of passages were blocked to study the effect of changes in the effective forward wall geometry and air flow distribution on combustor performance.

In order to accommodate the turning vanes, a new combined diffuser-flameholder (CDF-2) was constructed with the same air flow split and inlet air flow trajectory as that of the ideal CDF configuration. All experiments run with the CDF-2 had the same cavity air loading and forward-to-aft air driver momentum ratio as that of the CDF configuration. Experiments were performed on the CDF-2 without vanes as a comparison to the baseline CDF configuration. This configuration without vanes had slightly lower inlet air velocities than the CDF configuration due to the lack of the blockage from the vanes. Experiments were also performed on the CDF-2 with vanes (CDF-2 V) to assess the vane's impact on combustion efficiency and exit temperature profile. The vanes had an axial length that was a factor of 2.0 greater than the combustor inlet height (*H*) and were designed to turn the flow 40 deg. It was anticipated that the low-pressure regions that form around the vane aid in mass transport from the cavity into the core flow. The vanes were water-cooled to ensure their survival at the high-temperature conditions.

Fuel (JP-8) was injected into the cavity along the forward face through six pressure atomizers for all configurations. A row of air jets was placed below the fuel injectors along the forward face. A second row of air jets was placed along the aft wall of the cavity (see Figs. 2 and 3). These air jets help to promote mixing of the fuel and air and drive a large vortex within the cavity. The diameter of the air driver jets were adjusted between experiments to provide different air loadings and momentum ratios between the air jets. The pressure drop of the fuel through the atomizer was nominally between 300 and 2600 kPa (45–380 psia), based on the desired equivalence ratio within the cavity.

Experiments were conducted at 520–1040 kPa (75–150 psia) and inlet temperatures equal to 480–620 K (865 R–1120 R). For brevity, only measurements made at 690 kPa (100 psia) and an inlet temperature equal to 530 K (960 R) are reported, unless otherwise noted.

Measurements. Three emissions rakes were located between the trailing edges of the deswirling vanes (see Fig. 2(*a*)) and used to pull exhaust samples to the gas analyzers. Each rake had five gas-sampling probes distributed across the height of the combustor. Nondispersive infrared analyzers (X-STREAM, X2GP), chemiluminescent (Eco Physics, CLD 700 AL), and flame-ionization detectors (Beckman, 402) were used to measure the concentration of carbon dioxide and carbon monoxide, NO_x, and total unburned hydrocarbons, respectively. The uncertainty of the emission rake measurements is ±3%, based on manufacturer specifications. The measurements were used to establish the combustion efficiency of each configuration and determine the exit temperatures, assuming chemical equilibrium. Combustion efficiency represents the portion of the carbon in the fuel that is converted into carbon dioxide. The probes were water-cooled to protect the instrumentation and to help quench the combustion products within the sampling elements. The overall combustion efficiency and NO_x emissions of the combustor were recorded by collecting samples from all 15 probes simultaneously (i.e., three rakes with five probes each). This produced a height and width-averaged sample of the combustion products. The reported temperature profiles were determined by averaging the temperatures (based on emission measurements) at the same height on all three rakes. Thus, the temperature profiles were width-averaged for the combustor. Reporting the global combustion efficiency and average temperature profile helped to reduce the impact of wall effects on the results and allowed for relative comparisons between different operating conditions.

Combustion efficiency is reported for various cavity equivalence ratios, forward-to-aft momentum ratios, and air loadings within the cavity. Air loading (*AL*) is defined as

$$AL = \frac{\dot{m}_{\text{air}}}{V_{\text{cavity}} \left(\frac{P_{\text{inlet}}}{101.325} \right)^{1.75} e^{\frac{T_{\text{inlet}}}{300}}} \tag{1}$$

where $\dot{m}_{\text{air}}$ is the air mass flow into the cavity in kg/s, V_{cavity} is the volume of the cavity in m^3, P_{inlet} is the plenum total pressure in kPa, and T_{inlet} is the plenum total temperature in Kelvin. An air loading of 1 kg/m^3-s is equal to 0.0624 lbm/ft^3-s. Increasing the air loading while maintaining a constant cavity equivalence ratio allows additional chemical energy to be released within the engine. However, excessive loading can lead to lower flame stability, poorer emissions profiles, and lower combustion efficiencies due to higher flame strain rates.

This effort consists of three sets of experiments used to ascertain key physics and operating constraints of the combustor. First, the number and location of the air passages on the CDF that allowed air to pass was varied. This allowed the interaction of cross-flow air jets with flow in the cavity to be better understood and the influence on combustor performance to be quantified. The average cavity air loading for these studies was 6.9 kg/s-m^3. Four variations were studied: the row of holes farthest from the cavity was open (*Pa*1top), the middle row of holes was open (*Pa*1middle), the row of holes nearest the cavity was open (*Pa*1bottom), and the middle and bottom rows of holes (i.e., nearest the cavity) were open (*Pa*2b + m), as illustrated in Fig. 3. In the second set of experiments, the forward-to-aft momentum ratio of the air jets in the cavity was similar and the cavity air loading was varied to ascertain the influence on combustor performance.

Table 1 presents the conditions for this second set of experiments (i.e., E1.x). The bottom row of holes on the CDF was open (*Pa*1bottom), and the remaining holes were blocked. In the third set of experiments, the *Pa*1bottom configuration of the CDF was validated against a similar front end without vanes (CDF-2). This CDF-2 was then compared to a configuration with vanes installed (CDF-2 V, Fig. 2). These experiments allowed for a comparison of the combustor performance and temperature profile between configurations that used just a CDF front end or used a CDF and vane combination (i.e., UCC) for cavity-core mixing. The air loading in the cavity for all cases were matched, and the forward-to-aft momentum ratio was 0.9. Other work has indicated that momentum ratios greater than or roughly equal to one in the cavity result in the highest combustion efficiencies.

Visible images indicated that the shape of the vortex observed within the cavity correlated with combustion efficiency. In an effort to quantify this observation, high-speed (i.e., 20-kHz) images of the visible flame radiation emitted from the cavity were processed using coherent-structure velocimetry to obtain path-averaged estimates of the gas velocities [17]. The relative

Table 1 Combustion parameters for studying influence of air loading on combustion efficiency. The bottom row of holes on the CDF was open.

	E1.1	E1.2	E1.3
Air loading (kg/s-m^3)	6.85	5.31	4.03
Forward-to-aft momentum ratio	0.92	0.89	1.00

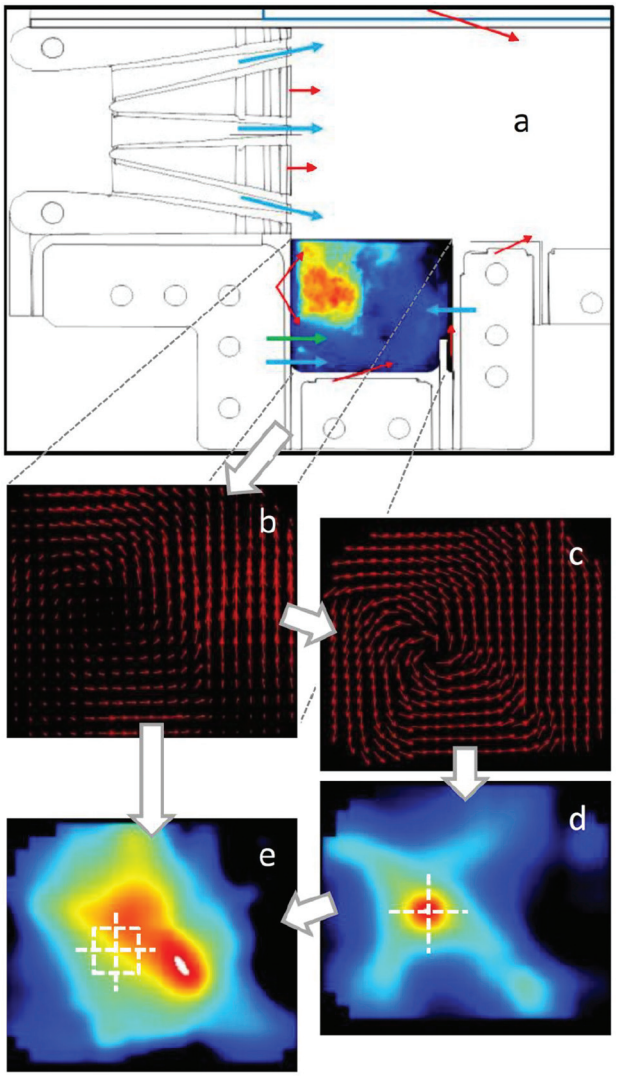

Fig. 4 Illustration of steps used to quantify vortex strength: (*a*) false color image of flame luminosity from high-speed movie showing location of air jets in blue, fuel injector in green, and effusion cooling in red; (*b*) representative gas velocities within combustor cavity based on coherent structure velocimetry; (*c*) magnitude-independent velocities; (*d*) magnitude-independent vorticity map showing location of vortex center, and (*e*) magnitude-dependent vorticity map and sample region used to find average vorticity value

strengths of the vortices in the cavity for different experimental configurations were compared by analyzing the velocities. The results of absolute gas-velocity measurements are not reported because of the path-averaged nature of the measurements and the complex three-dimensional nature of the flow within the cavity.

Figure 4 illustrates the image-processing steps used to determine the strength of the large vortex observed within the cavity. Consecutive images from the high-speed image series (e.g., Fig. 4(*a*)) were employed to determine a two-dimensional velocity field using standard particle image velocimetry cross-correlation functions. A multipass algorithm was used with the final subimage size of 32×32 pixels. The resulting vector field was smoothed and filtered based on the variance of nearby vectors. Figure 4(*b*) shows representative calculated velocity fields. These vectors ($\boldsymbol{u}$) of the form

$$u_{ij} = u_x\hat{i} + u_y\hat{j} \tag{2}$$

were normalized by their respective magnitudes ($|u|$) to produce a unit vector field,

$$\tilde{u}_{ij} = \frac{u_{ij}}{|u_{ij}|} \tag{3}$$

This approach preserves only the directionality of the vectors. Figure 4(*c*) displays a typical magnitude-independent velocity vector field. Once the unit vector field was obtained, the magnitude-independent vorticity,

$$\vec{\mu} = \frac{\partial \tilde{u}_y}{\partial x} - \frac{\partial \tilde{u}_x}{\partial y} \tag{4}$$

was calculated at every point using Eq. (4), as illustrated in Fig. 4(*d*). The location of maximum magnitude-independent vorticity ($\vec{\mu}$) was identified as the center of the vortex; indeed, this was the location in the flow where the streamlines approximately formed a circle, as would be expected at the center of a vortex. Using the magnitude-independent vorticity to locate the vortex center yielded the best agreement with visual inspection of the high-speed images. Attempts to use the magnitude-dependent vorticity ($\vec{\xi}$) to identify the center were biased because the location of maximum magnitude-dependent vorticity occurred in the shear layer outside the vortex.

With the center of the vortex determined, the magnitude-dependent vorticity,

$$\vec{\xi} = \frac{\partial u_y}{\partial x} - \frac{\partial u_x}{\partial y} \tag{5}$$

was calculated using Eq. (5) and the velocity field from Eq. (2). The vortex strength (Ξ) is defined as the average of the magnitude-dependent vorticity in a 25×25 square pixel region centered at the vortex center (denoted as white dashed rectangle in Fig. 4(*e*)). This pixel window size was chosen because it accounts for the rotational vorticity of the vortex core and excludes the majority of the shear-generated vorticity of the aft air jets. The vortex strengths reported later in this paper are the average from 1000 consecutive high-speed images for each configuration.

Results and Discussion

This section addresses three aspects of a UCC: (1) the sensitivity of combustor performance to changes in the distribution of core-flow air into the combustor, (2) the cavity air-loading range over which the combustor can be operated, and (3) the impact of the CDF (i.e., distributed core flow air) or turbine inlet vanes on combustion efficiency and temperature profiles. Changes in the fluid mechanics and combustion properties are discussed for the three aspects.

Interaction With Combined Diffuser-Flameholder. Experiments were performed to aid in understanding the impact of discrete jets of air entering the front of the combustor on combustor performance. Comparisons of combustion efficiency, NO_x emissions, and profile factors were made with the top (i.e., *Pa*1top), middle (i.e., *Pa*1middle), bottom (*Pa*1bottom), and bottom and middle (*Pa*2b + m) rows of holes open on the CDF. The data serve as a baseline for comparisons when a vane is present, as discussed in the next section.

The combustion efficiency and vortex strength for the various CDF configurations are shown in Fig. 5. The forward-to-aft momentum ratios were nominally 0.9, and the cavity-air loadings were 7 kg/s-m^3. The configurations with the bottom row of holes open (*Pa*1bot and *Pa*2b + m) had combustion efficiencies >99% for $\Phi_{cavity} < 1.3$. The configurations with the bottom row of holes closed (*Pa*1top and *Pa*1mid) had a narrower range (i.e., $\Phi_{cavity} < 1.0$), over which similar combustion efficiencies were observed. It was noted that the configurations with the bottom row of holes open tended to have higher combustion efficiencies at

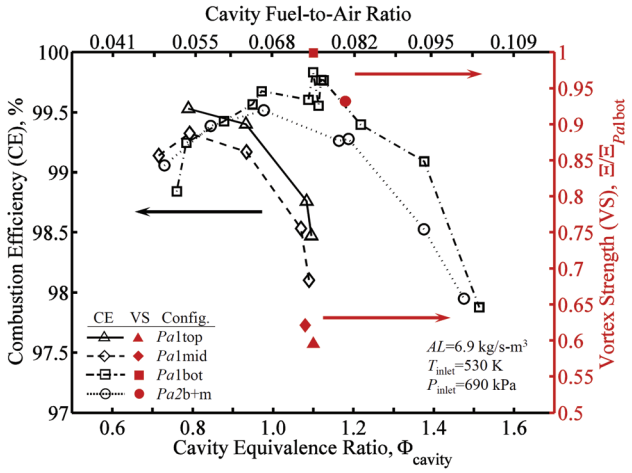

Fig. 5 Combustion efficiency and normalized vortex strength as a function of cavity equivalence ratio for the top (*Pa*1top), middle (*Pa*1middle), bottom (*Pa*1bottom), and bottom and middle (*Pa*2b + m) rows of passages open on CDF

similar cavity equivalence ratios than configurations without the bottom row of holes open. These results show that the interaction of the bottom row of air jets with the fluid within the cavity has a beneficial effect on the combustion process.

The vortex strength is plotted on Fig. 5 for comparison and to provide insight into changes in the fluid mechanics within the cavity. The vortex strength was highest for the combustor configurations with the bottom row of holes of the CDF open (i.e., *Pa*1bot and *Pa*2b + m); these configurations also had the highest combustion efficiencies. The former configuration, which had the peak combustion efficiencies, had a vortex strength that was 7% higher than that of the latter. The two configurations with the bottom row of holes blocked on the CDF (and the lowest combustion efficiencies) had vortex strengths which were ~40% less than that of the configuration with the bottom row of holes open. These observations indicate that the bottom row of CDF air jets reinforces the vortex within the cavity. It is plausible that stronger vortical structures improve combustion efficiency by enhancing mixing between the fuel and air and increasing the residence time within the cavity for completing reactions.

Figure 6 displays emission indices of NO_x corresponding to the test results reported in Fig. 5. The configurations with the lowest combustion efficiencies and the smallest vortex strength (i.e., bottom passage closed) have the highest NO_x emissions ($4.5 < EINO_x < 6.5$ g/kg$_{fuel}$). Conversely, the configurations with the highest combustion efficiencies and greatest vortex strength (i.e., bottom passage open) have the lowest NO_x emissions (at an equivalent Φ_{cavity}).

Normalized exit temperature profiles for the various CDF configurations are reported in Fig. 7. The temperature profiles were obtained in between the trailing edge of the deswirler vanes. The general trend of the normalized temperature profiles was similar for the various configurations of the CDF. Peak temperatures were observed for $0.3 < y_c/H < 0.5$, where $y_c = 0$ corresponds to the cavity-side liner and $y_c = 1$ to the opposite-side liner (see Fig. 3). Separation of the peak temperature from the cavity-side liner (i.e., $y_c/H = 0$) results from fuel-rich combustion products being transported from the cavity along the face of the CDF and reacting with the discrete jets of air. The lowest temperature occurs near the liner opposite the cavity (i.e., $y_c/H = 0.9$); this is expected, since combustion products from the cavity must propagate farthest to this location. The configuration with the row of CDF holes open nearest the cavity (*Pa*1bot) exhibited the most uniform temperature distribution. The temperature varied within 15% of the mean. In the other configurations, the temperature varied by as much as 30% with respect to the mean.

Cavity Air Loading. The sensitivity of combustion efficiency to changes in air loading was measured for the configuration with the bottom row of air holes open along the CDF. This configuration was chosen because it typically had the highest combustion efficiencies at equivalence ratios greater than unity. The diameter of the air holes on the cavity was varied between configurations to allow greater air loadings in the cavity (i.e., greater air mass flows), while the forward-to-aft momentum ratio was fixed between 0.9 and 1. Configuration E1.1 had the highest average air loading and E1.3 had the lowest (see Table 1).

Contour plots of combustion efficiency for different cavity equivalence ratios and air loadings are shown in Fig. 8. The contour lines and colors in the figure are interpolated from the data (points) and represent levels of combustion efficiency varying from 96% (blue) to 100% (red). The configuration with the highest average air loadings (E1.1) had combustion efficiencies >99% for $0.8 \le \Phi_c \le 1.4$ and for $4.8 < AL < 9.6$ kg/m^3-s. In contrast, the configuration with the lowest average air loading (E1.3) had similar combustion efficiencies for $0.9 \le \Phi_c \le 1.7$ and for $3.2 < AL < 6$ kg/m^3-s. To summarize, as the air loading was increased, the range of cavity equivalence ratios over which combustion efficiencies are greater than 99% shifted toward lower

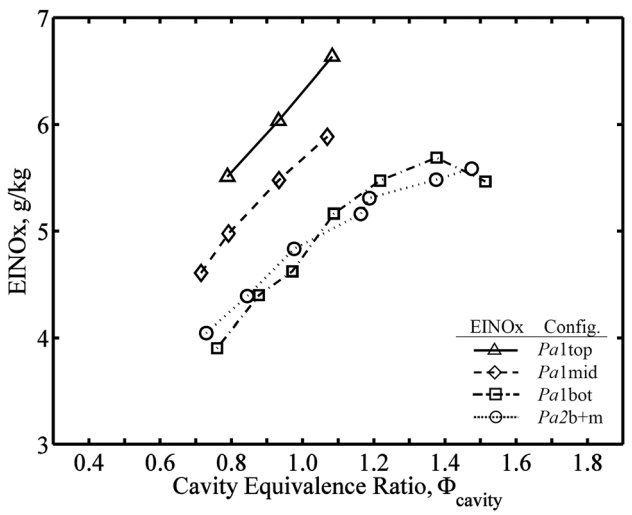

Fig. 6 Emission indices of NO_x for experiments corresponding to combustion efficiencies reported in Fig. 7

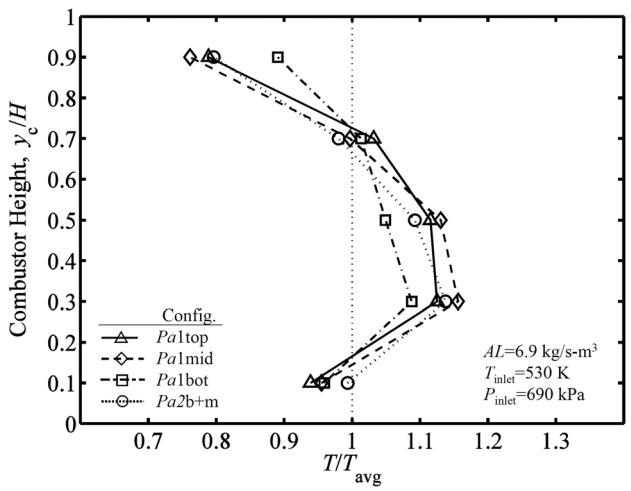

Fig. 7 Normalized exit temperature profiles for testing with different rows of holes on CDF open

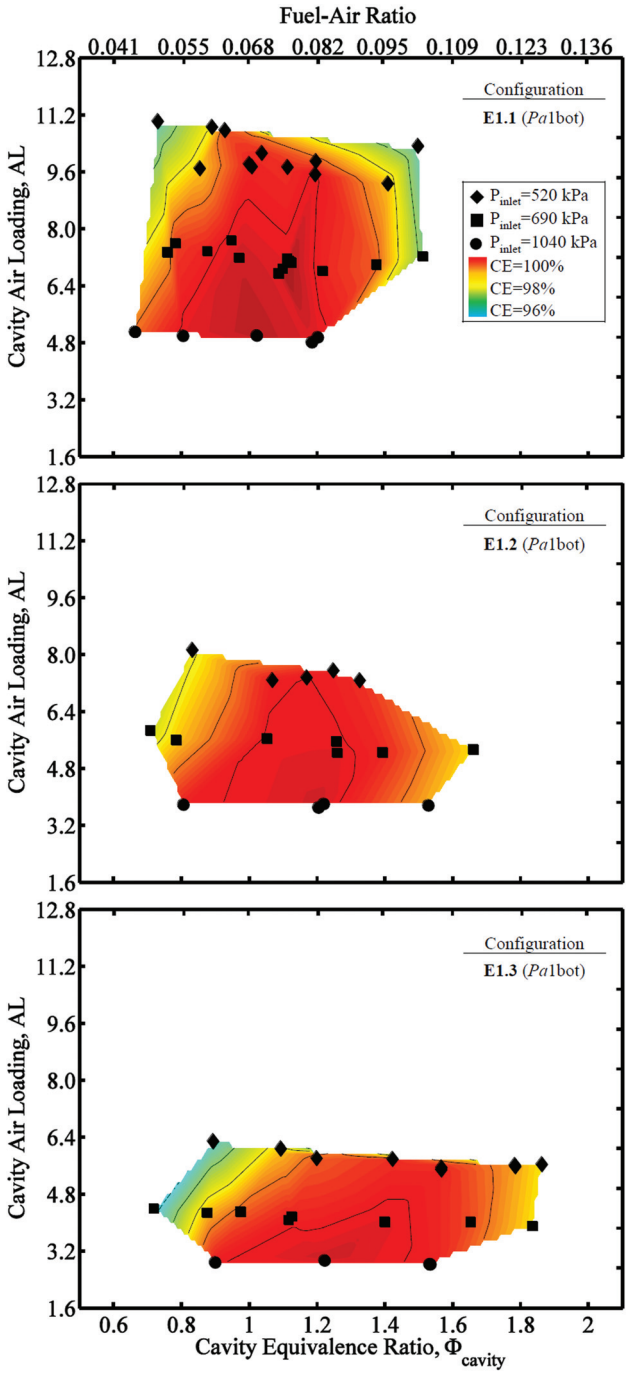

Fig. 8 Combustion efficiency (colored contours) as cavity air loading and cavity equivalence ratio were varied for configurations with bottom row of air jets open along the CDF (*Pa*1bot). The three panels correspond to different inlet areas of the driver jets in the cavity.

values and became narrower. The contour plots illustrate a trade-off between cavity air loading and cavity equivalence ratio as the region of highest combustion efficiency widens at lower air loadings and narrows at higher air loadings.

The combustion efficiency in Fig. 8 corresponding to testing at an inlet pressure of 690 kPa is plotted with respect to the fuel mass flow rate in Fig. 9. The corresponding vortex strength is included in the plot. Recall that increasing the air loading requires an increase in fuel mass flow rate for a constant cavity equivalence ratio. As the air loading was increased, the range of fuel mass flows over which combustion efficiencies exceed 99%

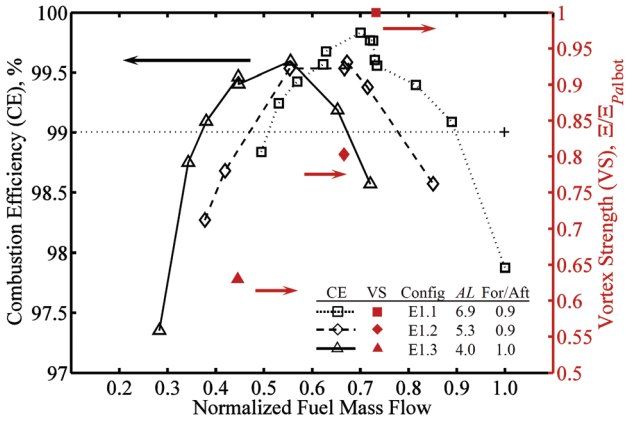

Fig. 9 Combustion efficiency for three air loadings and bottom row of holes on CDF open

shifted toward higher values and became wider. Configuration E1.1 (i.e., highest air loading) had combustion efficiencies >99% for normalized fuel mass flows between 0.5 and 0.9. Conversely, configuration E1.3 (i.e., lowest air loading) had similar efficiencies for normalized fuel mass flows between 0.4 and 0.7. For combustor control over a wide range of engine-operating conditions, the combustion efficiency must remain sufficiently high for a wide range of fuel mass flows. Configuration E1.1 exhibits the widest turndown ratio but suffers at lower power conditions. Configuration E1.3 has a smaller operating range but performs better at lower power.

The vortex strength varied significantly among the three air loadings, with the lowest vortex strength correlating with the lowest air loading (E1.3), the medium with the middle air loading (E1.2), and the highest with the highest air loading (E1.1). Indeed, configurations E1.1 had a 70% higher air loading for a nearly 60% higher vortex strength than configuration E1.3. The higher air loading increases the momentum of the air jets entering the cavity and reinforces the large vortex within the cavity.

Figure 10 displays emission indices of NO_x corresponding to the results reported in Figs. 8 and 9. The emissions generally increase monotonically with respect to the cavity equivalence ratio. Minimum NO_x emissions ($\sim$3.5 g/kg$_{fuel}$) were observed near cavity equivalence ratios equal to 0.7, while peak values ($\sim$6 g/kg$_{fuel}$) were observed near a cavity equivalence ratio equal to 1.6. Increasing the cavity equivalence ratio increased the fuel-to-air ratio and the temperature within the combustor.

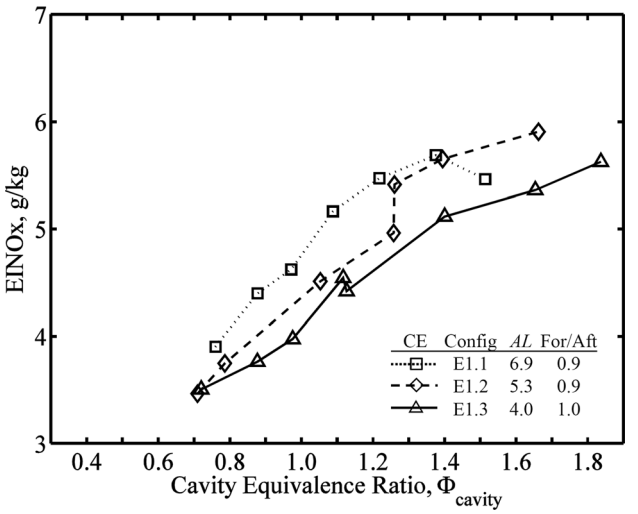

Fig. 10 Emission indices of NO_x for three air loadings and bottom row of holes on CDF open (E1.x)

Turning Vanes. The *Pa*1bot arrangement of the CDF, which had the best combustion efficiencies, was used as a guide for designing a modified CDF (i.e., CDF-2), which allowed the incorporation of turning vanes (i.e., CDF-2 V). This enabled comparison of combustion performance for the original and updated CDF configurations and a UCC with a vane.

The combustion efficiencies for testing performed using the three configurations are shown in Fig. 11. The combustion efficiency for the CDF-2 was comparable to that of the CDF at a $\Phi_{cavity} = 0.7$ and slightly higher at $\Phi_{cavity} = 1.1$. The results indicate that the combustor performance was similar using the two CDF designs for the limited data points for comparison (due to experimental limitations). This was not surprising considering that both configurations are designed to have the same fluid mechanics within the cavity by having the core flow across the top of the cavity through discrete jets.

With confidence in the modified CDF design, turning vanes were incorporated into the combustor. The combustion efficiency for CDF-2 V, as shown in Fig. 11, was greater than the original CDF configuration for all cavity equivalence ratios and greater than or equal to the results for the CDF-2 arrangement. Combustion efficiencies greater than 99.5% are observed over the entire range of cavity equivalence ratios tested ($0.8 \leq \Phi_{cavity} \leq 1.8$). The greater range of cavity equivalence ratios tested was enabled by water cooling of the vanes and confidence in the survivability of the combustor. The improved combustion efficiency with the inclusion of vanes is attributed to the development of vortical structures, which enhance mixing of the cavity products with the cross-flowing air. Note that the vortex strength is not reported for comparison. Visible observations of the flame indicated that the vortex strength may not be an appropriate metric for quantifying the apparent fluid mechanics within the cavity for the configurations beyond the baseline CDF.

The temperature profiles of the CDF (*Pa*1bot), CDF-2, and CDF-2 V configurations are shown in Fig. 12 for comparison. Both the CDF-2 and CDF-2 V configurations had temperature profiles which were within 10% of the mean value, whereas the CDF configuration had a profile within 12%. The CDF-2 configuration had a higher peaked profile at 70% height, whereas the CDF and CDF-2 V configurations were peaked at 30%. The greater height of the peak temperature for the CDF-2 configuration indicates that hot combustion products from the cavity penetrate farther into the cross flow. These results are surprising, considering that vanes should enhance mass transport from the cavity (due to pressure gradients), yet this is not observed. This requires further investigation

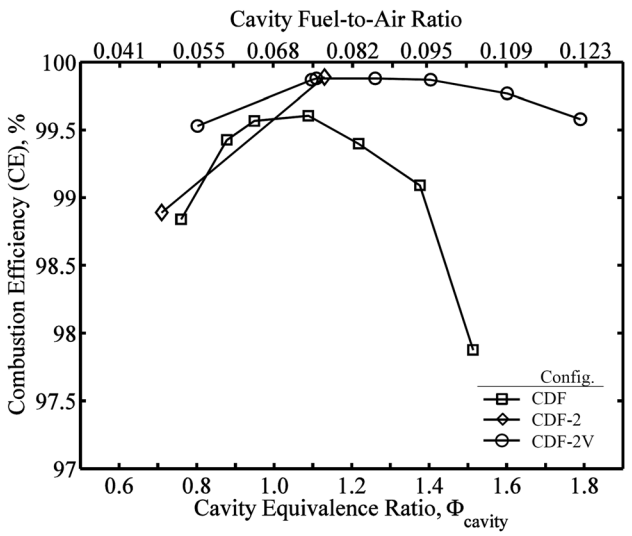

Fig. 11 Combustion efficiency as a function of cavity equivalence ratio for the *Pa*1bot CDF, the CDF-2, and the CDF-2 with vanes configurations

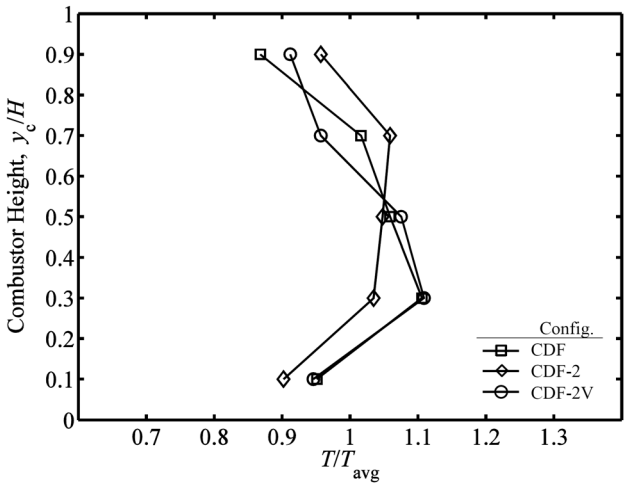

Fig. 12 Normalized exit temperature profile for testing with the Pa1bot CDF, the CDF-2, and the CDF-2 with vanes configurations

and is beyond the scope of the current effort. The ±12% variation in the temperature profile for the three configurations may be manageable for turbine inlet temperatures but does not achieve an optimal 50% temperature peak. In an effort to increase penetration of exhaust products from the cavity into the core flow and improve the temperature profiles, Briones et al. [4,18] numerically investigated vane designs with notches or dimples included on the suction side of the vane. Improvements in the temperature profiles relative to a smooth vane (current work) were predicted for several configurations. The improvements are attributed to the notches or dimples creating localized regions with lower pressure along the vane and improving mixing and mass transport from the cavity into the core flow.

Conclusions

A trapped-vortex UCC was used to study the effect of inlet air distribution, air loading, and turning vanes on combustion efficiencies, exit temperature profiles, and NOx emissions. Higher combustion efficiencies typically corresponded to greater vortex strengths, as measured by coherent structure velocimetry of combusting gases in the cavity when the CDF is used. Well-developed vortical structures enhance mixing between the fuel and air and increase the residence time, thus increasing the combustion efficiency. Emission indices of NO_x were between 3.5 and 6.5 g/kg_{fuel} for all test conditions.

Increasing the cavity air loading decreases the range of cavity equivalence ratios where peak combustion efficiencies are observed. However, increasing the air loading enabled greater mass flow rates of fuel (i.e., chemical energy release) with equivalent combustion efficiencies.

Discrete jets of air immediately above the cavity opening (i.e., *Pa*1bottom) produce the highest combustion efficiencies as a result of strengthening the vortex trapped within the cavity. The temperature distribution at the combustor exit is more uniform (i.e., within 10% of average) for this configuration than for those with a vane (i.e., within 30% of average). This is a result of the discrete jets of air and the bluff-body nature of the CDF aiding in transport of the combustion products out of the cavity. Testing with a vane and a similar front-end configuration showed a 10% variation in the temperature profile with respect to the mean. Including a turning vane led to an increase in the combustion efficiencies for a broader range of cavity equivalence ratios.

Acknowledgment

Brad Day, Justin Inman, Dave Baker, and Ron Britton (Innovative Scientific Solutions, Inc. (ISSI)) helped with data collection.

Jack Yoder, also from ISSI, provided the combustor drawings. Ryan Battelle (AFRL) performed the cycle analysis. Marion Whitaker aided in revising the manuscript. Rebecca Howard (UTC) integrated diffusor studies supportive of this work. Pete Koch (AFRL) aided in the design of the turbine inlet vane that was placed in the combustor. This material is based on research sponsored by the Air Force Research Laboratory under contract nos. FA8650-10-2-2934 and F33615-03-D-2329. The U.S. Government is authorized to reproduce and distribute reprints for governmental purposes notwithstanding any copyright notation thereon. The views and conclusions contained herein are those of the authors and should not be interpreted as necessarily representing the official policies or endorsements, either expressed or implied, of the Air Force Research Laboratory or the U.S. Government.

Nomenclature

AL = air loading within cavity
CDF = combined diffuser-flameholder
CE = combustion efficiency
D = cavity depth
d_{exit} = diffuser exit height
d_{inlet} = diffuser inlet height
H = height of combustor inlet
ITB = interturbine burner
$\dot{m}_{\text{air}}$ = air mass flow rate
$\dot{m}_{\text{fuel}}$ = fuel mass flow rate
OGV = compressor outlet guide vane
P_{inlet} = inlet pressure
Pa = air passage through CDF
T = temperature
T_{avg} = average temperature
T_{inlet} = inlet temperature
TVC = trapped-vortex combustor
u = velocity vector
UCC = ultracompact combustor
V_{cavity} = volume of cavity
VS = vortex strength
W = width of cavity
y_c = vertical distance from top of cavity

Greek Symbols

ξ = vorticity (magnitude-dependent)
μ = vorticity (magnitude-independent)
Ξ = average value of magnitude-dependent vorticity
Φ_{cavity} = equivalence ratio in cavity

References

[1] Briones, A., Zelina, J., and Katta, V., 2010, "Flame Stabilization in Small Cavities," AIAA J., **48**(1), pp. 224–235.
[2] Briones, A. M., Thornburg, H., Sekar, B., Neuroth, C., and Shouse, D., 2013, "Numerical-Experimental Research of Ultra Compact Combustors Containing Film and Effusion Cooling," 51st AIAA Aerospace Science Meeting, Grapevine, TX, January 7–10, AIAA Paper No. 2013-1045.
[3] Anderson, W., Radtke, J., King, P., Thornburg, H., Zelina, J., and Sekar, B., 2008, "Effects of Main Swirl Direction on High-g Combustion," 44th Joint Propulsion Conference, Hartford, CT, July 21–23, AIAA Paper No. 2008-4954.
[4] Briones, A., Sekar, B., Thornburg, H., and Zelina, J., 2010, "Effect of Vane Notch and Ramp Design on the Performance of a Rectangular Inter-Turbine Burner," 48th AIAA Aerospace Sciences Meeting, Orlando, FL, January 4–7, AIAA Paper No. 2010-581.
[5] Kostka, S., Branam, R. D., Renfro, M. W., Lakusta, P. J., Gord, J. R., and Roy, S., 2012, "Laser-Induced Fluorescence Measurements of Product Penetration Within an Ultracompact Combustor," J. Propuls. Power, **23**(3), pp. 617–624.
[6] Zelina, J., Shouse, D., Stutrud, J., Sturgess, G., and Roquemore, W., 2006, "Exploration of Compact Combustors for Reheat Cycle Aero Engine Applications," ASME Turbo Expo, Barcelona, Spain, May 8–11, ASME Paper No. GT2006-90179.
[7] Blunck, D., Shouse, D., Neuroth, C., Battelle, R., Lynch, A., Sekar, B., Zelina, J., Erdmann, T., Burrus, D., Howard, R., Briones, A., Richardson, D., and Caswell, A., "Experimental and Computational Studies of an Ultra-Compact Combustor," ASME Turbo Expo, San Antonio, TX, June 3–7, ASME Paper No. GT2013-94372.
[8] Sirignano, W., and Liu, F., 1999, "Performance Increases for Gas-Turbine Engines Through Combustion Inside the Turbine," J. Propuls. Power, **15**(1), pp. 111–118.
[9] Cheng, F., Liu, F., and Sirignano, W., 2007, "Nonpremixed Combustion in an Accelerating Transonic Flow Undergoing Transition," AIAA J., **45**(12), pp. 2935–2946.
[10] Zelina, J., Shouse, D., and Neuroth, C., 2005, "High-Pressure Tests of a High-g, Ultra-Compact Combustor," 41st AIAA/ASME/SAE/ASEE Joint Propulsion Conference, Tucson, AZ, July 10–13, AIAA Paper No. 2005-3779.
[11] Zelina, J., Anderson, W., and Shouse, D., 2008, "Compact Combustion Systems Using a Combination of Trapped Vortex and High-G Combustor Technologies," 53rd ASME International Gas Turbine and Aeroengine Congress and Exposition, Berlin, June 9–13, ASME Paper No. GT2008-50090.
[12] Sturgess, G., and Hsu, K., 1997, "Entrainment of Mainstream Flow in a Trapped-Vortex Combustor," 35th AIAA Aerospace Sciences Meeting, Reno, NV, January 6–9, AIAA Paper No. 1997-0261.
[13] Sturgess, G., Zelina, J., Shouse, D., and Roquemore, W., 2005, "Emissions Reduction Technology for Military Gas Turbine Engines," J. Propuls. Power, **21**(2), pp. 193–217.
[14] Burguburu, J., Cabot, G., Renou, B., and Boukhalfa, A. M., 2012, "Flame Stabilization by Hot Products Gases Recirculation in a Trapped Vortex Combustor," ASME Turbo Expo, Copenhagen, Denmark, June 11–15, ASME Paper No. GT2012-68451.
[15] Bohan, B. T., and Polanka, M. D., 2011, "Analysis of Flow Migration in an Ultra-Compact Combustor," ASME Turbo Expo, Vancouver, Canada, June 6–10, ASME Paper No. GT2011-45916.
[16] Sekar, B., Thornburg, H., Briones, A., and Zelina, J., 2009, "Effect of Trapped Vortex Combustion With Radial Vane Cavity Arrangements on Predicted Inter-Turbine Burner Performance," 7th International Energy Conversion Engineering Conference, Denver, CO, August 2–5, AIAA Paper No. 2009-4603.
[17] Meyer, T. R., Brown, M. S., Fonov, S., Belovich, V. M., Roquemore, W. M., Goss, L. P., Cooper, C. S., Gord, J. R., Shouse, D. T., Kim, E. S., and Haynes, J. M., 2002, "Optical Diagnostics and Numerical Characterization of a Trapped-Vortex Combustor," 38th AIAA/ASME/SAE/ASEE Joint Propulsion Conference and Exhibit, Indianapolis, IN, July 7–10, AIAA Paper No. 2002-3863.
[18] Briones, A., Sekar, B., and Thornburg, H., 2011, "Enhanced Mixing in Trapped Vortex Combustor With Protuberances Part 2: Two-Phase Reacting Flow," 41st AIAA Fluid Dynamics Conference and Exhibit, Honolulu, HI, June 27–30, AIAA Paper No. 2011-3422.